



Transfer and Amplification of Chirality Within the “Ring of Fire” Observed in Resonance Raman Optical Activity Experiments

Guojie Li, Jiří Kessler, Joseph Cheramy, Tao Wu, Mohammad Reza Poopari, Petr Bouř,* and Yunjie Xu*

Abstract: We report extremely strong chirality transfer from a chiral nickel complex to solvent molecules detected as Raman optical activity (ROA). Electronic energies of the complex were in resonance with the excitation-laser light. The phenomenon was observed for a wide range of achiral and chiral solvents. For chiral 2-butanol, the induced ROA was even stronger than the natural one. The observations were related to so-called quantum (molecular) plasmons that enable a strong chiral Rayleigh scattering of the resonating complex. According to a model presented here, the maximal induced ROA intensity occurs at a certain distance from the solute, in a three-dimensional “ring of fire”, even after rotational averaging. Most experimental ROA signs and relative intensities could be reproduced. The effect might significantly increase the potential of ROA spectroscopy in bioimaging and sensitive detection of chiral molecules.

Most important molecules in living organisms are chiral and thus sensitive to circularly polarized light. This sensitivity was first explored by Pasteur,^[1] and since then an amazing variety of chiroptical methods has been developed for fundamental studies and practical applications.^[2] One of the youngest and most dynamically evolving tools is Raman optical activity (ROA).^[3] It can provide rich stereochemical information because of the large number of vibrational bands usually exhibited by chiral molecules, and is directly applicable to solutions.

However, the ROA effect is weak, and a large amount of the sample is usually needed for the analysis. This has prompted vigorous searches for enhancement techniques, utilizing, for example, molecular resonance,^[4] nanoplasmons (resonating metallic nanoparticles),^[5] and molecular aggregation.^[6] Interesting phenomena such as ROA induction in achiral reporter molecules in the presence of nanoplasmons or a solvent-signal enhancement under hyper-Raman scattering have been observed.^[5c,7,8] Even though many properties of the nanoplasmons can be explained by established electro-

magnetic and chemical theories,^[9] the ROA enhancement and many chirality-transfer effects have so far resisted detailed interpretation.

In this context, we believe that the strong chirality transfer under resonance conditions described in this work significantly contributes to the understanding of molecular interactions with chiral light. We report strong ROA of a range of solvents induced by a chiral nickel complex under resonance conditions. Contrary to common belief, the chirality transfer appears quite general, and the induced ROA signals were even stronger than those of the Ni complex itself. For 2-butanol, a chiral solvent, the induced ROA intensity was stronger than the natural one.

The resonance-ROA phenomenon itself, an area of intense experimental and theoretical interest, can be rationalized only in simple cases.^[4a,10] None of them, however, is applicable to the observations presented here. Based on extensive experimental data and model calculations, we show that the effect is not caused by specific chemical bonding, π - π stacking, and/or hydrogen bonding, but rather based on through-space solvent-solute interactions, a concept utilized for describing, for example, chirality transfer in the presence of nanoplasmons.^[5a]

This outcome is surprising because the Ni complex molecule is much smaller than nanoparticles. However, in resonance with laser radiation, its polarizability significantly increases. The results thus can be linked to so-called quantum plasmons,^[11] a term used to describe plasmonic behavior at the molecular limit. One may therefore expect further fundamental and practical explorations in this area.^[12]

The Ni complex itself (Figure 1) was previously investigated by UV/Vis and IR absorption spectroscopy, electronic and vibrational circular dichroism (ECD, VCD), and density functional theory (DFT).^[13] The UV/Vis and ECD spectra contain several bands and can be reasonably well explained on the basis of time-dependent DFT (Figure S1, Supporting Information). Interestingly, the first three lowest-energy transitions with a strong participation of nickel d-orbitals ($S_0 \rightarrow S_1$, $S_0 \rightarrow S_2$, and $S_0 \rightarrow S_3$) show relatively high dissymmetry factors g (CD-to-absorption ratio, up to $g = 0.0762$, see also Table S1 and S2, and Figures 1 A and S2). These g -values are about 100 times larger than those for common chiral molecules.

As schematically shown in Figure 1 A, the equilibrium geometries of the three lowest-energy excited electronic states differ significantly from that of the ground state. Therefore, the ground-state vibrational wavefunction overlaps with a large number of excited vibrational states. The vibrational sub-structure of the electronic bands is not

[*] G. Li, Dr. J. Cheramy, Dr. M. R. Poopari, Prof. Y. Xu
Department of Chemistry, University of Alberta
Edmonton, Alberta, T6G 2G2 (Canada)
E-mail: yunjie.xu@ualberta.ca

Dr. J. Kessler, Dr. T. Wu, Prof. P. Bouř
Institute of Organic Chemistry and Biochemistry
Flemingovo náměstí 2, 16610 Prague (Czech Republic)
E-mail: bour@uochb.cas.cz

Supporting information and the ORCID identification number(s) for the author(s) of this article can be found under:
<https://doi.org/10.1002/anie.201909603>.

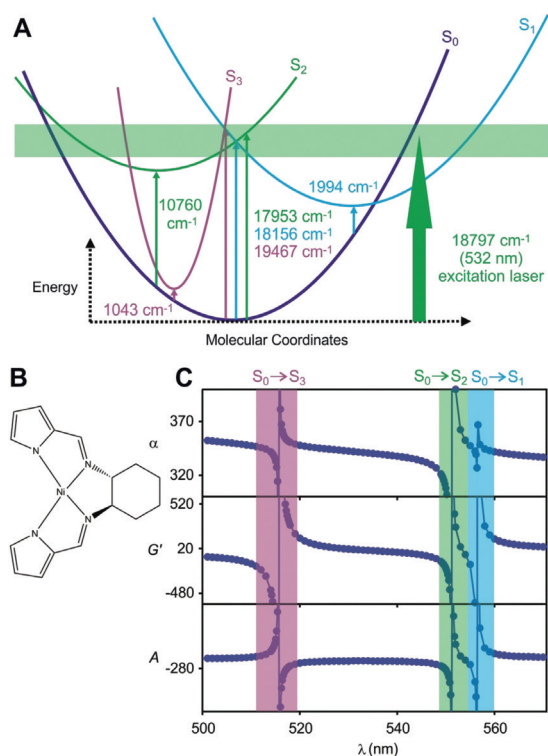


Figure 1. Structure and electronic states of the (*R,R*)-bis(pyrrol-2-ylmethyl)amine)cyclohexane nickel(II) complex, (*R,R*)-Ni. A) Simplified scheme of the first four singlet electronic states with transition energies in vicinity of the 532 nm laser excitation. B) Structural formula of the complex. C) Dependence of the ROA tensors (sums of the diagonal elements of α , G' , and A , in atomic units) on the excitation wavelength. The colored bars indicate the divergent regions. The CAM-B3LYP/6-311++G**/PCM/CHCl₃ method was used in the computations.

resolvable, which is consistent with the experimental UV/Vis and ECD spectra.^[13] When the excitation light is in resonance with these electronic transitions, molecular polarizabilities (and their derivatives determining Raman and ROA intensities) sharply increase. A typical dependence of the polarizability tensors α , G' , and A ^[2,3] on the wavelength can be seen in Figure 1C. Raman and ROA measurements also confirm the enhancement at 532 nm (resonance) when compared to laser excitations at 633 and 785 nm (non-resonance; Figure S3), and can be qualitatively reproduced by DFT computations (Figure S4). Minor inconsistencies are due to the limited accuracy of DFT^[14] and the pre-resonance approximation.^[3a]

While the behavior of the Ni complex fits into established theories, the accompanying huge ROA signal of the solvents was unexpected. Figure 2 shows the effect for CHCl₃/CDCl₃, DCM, dimethyl sulfoxide (DMSO and [D₆]DMSO), and mixtures containing benzene, acetone, methanol (MeOH and [D₄]MeOH), carbon tetrachloride (CCl₄), and acetonitrile ([D₃]ACN). This variety of polar/nonpolar, hydrogen-bond-donor/acceptor, and chlorinated solvents was chosen to test if the formation of long-lived chiral solute–solvent clusters^[15] was responsible for the chirality transfer.^[16] Despite significant differences in physical and chemical properties, such as

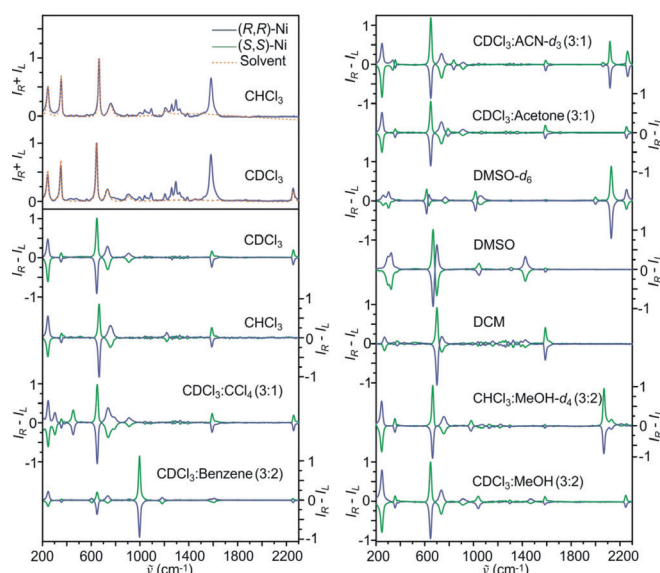


Figure 2. Experimental Raman ($I_R + I_L$) and ROA ($I_R - I_L$) spectra of the (*R,R*)- and (*S,S*)-Ni complexes in CHCl₃ and CDCl₃ solutions (top left) and ROA spectra in nine other achiral organic solvents or their mixtures. The intensity is normalized to the strongest peak in each trace, the circular intensity difference (ratio of ROA and Raman intensities) varied from 10^{-3} to 10^{-2} .

polarity, dielectric constant, hydrogen- or π -bonding capabilities, the effect was observed in all solvents. The solvent response is approximately linear so that the signal from a solvent mixture is a sum of the individual solvent components.

(*R*)- and (*S*)-2-butanol were investigated as solvents possessing natural (permanent) chirality. Despite the low solubility in 2-butanol, the addition of a small amount of the Ni complex altered the ROA spectra noticeably (Figure S5). The competition between induced and natural chirality is clearly visible, even though none of the Ni-complex ROA bands are apparent (Figure S5). In a 2-butanol/CDCl₃ solvent mixture, the complex is more soluble and its ROA bands, including the strongest one at 1588 cm⁻¹, become visible. More importantly, the (*R*)-2-butanol ROA bands exhibit the mirror-image symmetry for solutions containing the (*R,R*)-Ni and (*S,S*)-Ni complexes (Figure S6). Under such conditions, the induced chirality dominates and the natural one becomes immeasurably small.

Raman and ROA bands of the Ni complex in CDCl₃ and in DCM are essentially unchanged by the solvent variation (Figure S7). This is probably also true for other solvents, although the Ni complex bands are often weak and difficult to identify because of experimental noise and interference with the strong induced solvent bands.

DFT simulations of non-resonance and resonance ROA spectra of a large number of clusters consisting of the Ni complex and a few solvent molecules predicted a much smaller induced ROA than in case of the isolated Ni complex (not shown), which is in contrast to experimental findings. Thus, an electromagnetic mechanism is more probable in which the resonating Ni complex behaves in a similar fashion to plasmonic metal nanoparticles used in surface-enhanced

Raman scattering (SERS). Indeed, a transition-polarizability model (TPM, Figure S8)^[17] based on through-space solute–solvent interactions rationalizes the observed solvent-chirality induction in the vicinity of the resonating molecule to a big extent. Similar to SERS, the effective polarizability of a molecular solvent–solute pair is much larger than the sum of the polarizabilities of the individual molecules.^[2,17c,18] Interestingly, for the complex in resonance, the maximum effective (total) polarizability occurs at distances larger than the smallest solute–solvent separation. Solvent molecules in this “ring of fire” (Figure 3) contribute most to the measured

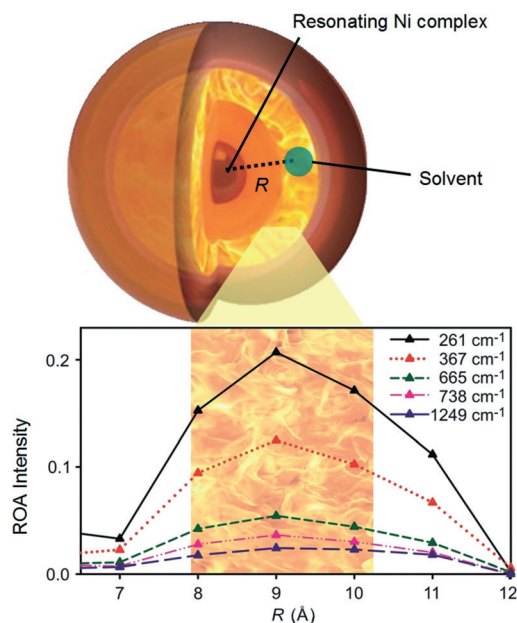


Figure 3. Suggested enhancement mechanism with the Ni complex at the center and a bright shell of solvent molecules contributing most to the induced ROA signal. The relative absolute intensity as a function of the distance between the Ni atom and the center of mass of CHCl_3 was calculated for five CHCl_3 vibrational transitions.

ROA spectra. The quantum plasmon—the Ni complex with large polarizabilities—thereby affects the properties of distant solvent molecules. Although the optimal distance cannot be computed accurately at the moment (a factor of 100 was assumed for the effective polarizabilities in Figure 3, compared to a non-resonance), it is clear that the volume around the solute and therefore the number of affected solvent molecules grows quite quickly with the distance ($\approx R^3$), and a strong spectroscopic response can be produced.

In Figure 4, we see a detailed comparison of the experimental and simulated induced ROA spectra of the solvents CHCl_3 , DCM, and DMSO in the presence of the (*R,R*)-Ni complex. Positions and assignments of the strongest bands for these and other solvents are listed in Table S3. In general, the TPM model reproduces the experimental sign patterns and major trends in relative induced ROA intensities. For DCM, for example, bands 1–3 are easily assigned, while bands 4–7 in the region of the Ni-complex signal can be identified based on the comparison done in Figure S7. Experimental signs and

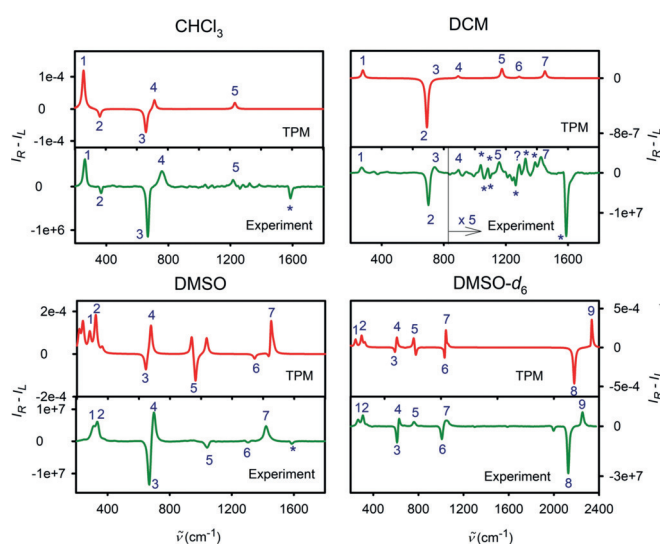


Figure 4. Examples of simulated and experimental induced ROA spectra. (*R,R*)-Ni complex bands are marked by an asterisk (*). Note that absolute intensities cannot be measured; therefore, the experimental (detector counts) and computed (atomic units) scales are not related.

relative intensities of bands 4, 5, and 7 also agree with the simulation, whereas band 6 overlaps severely with a Ni-complex band. For DMSO and $[\text{D}_6]\text{DMSO}$, some predicted ROA signals with frequencies near band 5 and below band 1 are not observed experimentally. However, the model cannot explain the observed high ROA/Raman ratios, probably caused by additional factors such as vibrational coherence or spin polarization.

Regarding the theoretical foundations of ROA, another surprising observation is that the electric-dipole/electric-quadrupole Rayleigh polarizability (A) is primarily responsible for the induced ROA event (Figure S9). As expected, the “ordinary” (achiral) α polarizability gives a zero contribution except for the anisotropic non-averaged case. But also the contribution of the G' tensor, which quite often dominates ROA spectra, is rather negligible when compared with A , confirming that the chirality-transfer mechanism here is different from regular molecular ROA.^[3a,19]

In conclusion, we have conducted several experiments showing that extremely strong chirality transfer under resonance is a common phenomenon. At least for the Ni complex, it was observed with a wide range of solvents and mixtures. For 2-butanol, the induced ROA was even stronger than the one caused by its natural chirality. The results indicate that the effect is caused by through-space solvent–solute interactions. The TPM model reproduced experimental ROA patterns well, although future work is needed to fully understand the observations. Apparently, the resonating Ni complex behaves like a quantum plasmon, where Rayleigh dipolar and quadrupolar electric and magnetic polarizabilities of the solute are greatly enhanced due to the resonance. The effect may open new opportunities for ROA spectroscopy for imaging and sensitive detection of biomolecules.

Experimental Section

Raman and ROA spectra were measured using a ChiralRaman-2X™ spectrometer (BioTools) operating with 532 nm laser excitation source. For a typical experiment, about 0.02 M or a saturated solution of the complex was used, with laser power at the source set to 30–50 mW and an accumulation time of \approx 25 h. Measurements with 633 nm and 785 nm excitation wavelengths were done on an inVia confocal Raman microscope (Renishaw). DFT calculations were performed with the Gaussian16 software package,^[20] using the B3LYP and CAM-B3LYP functionals and the 6-311++G(2df,2pd) basis set.^[21] The observed dependence on functional and basis set was consistent with previous studies.^[22] The solvent was modeled using the polarizable continuum model (PCM).^[23] In some computations, the LanL2DZ^[24] effective core potential and basis set were used for Ni. The B3LYP/6-311++G(2df,2pd)/PCM ROA polarizabilities (tensors α , G' , and A , see Ref. [2]) were used as input parameters for the TPM as described in Figure S8. Further experimental and computational details can be found in Supporting Information.

Acknowledgements

We thank Prof. M. T. McDermott and A. Y. Mahmoud for Raman measurements at 633 and 785 nm, and Dr. J. Cheeseman as well as Profs. J. Bloino, L. D. Barron, L. A. Nafie, and W. Jäger for discussions. This work was funded by the NSERC and CFI of Canada, Alberta Enterprise and Advanced Education, the University of Alberta, and GAČR and MŠMT of the Czech Republic (grant numbers 18-05770S, LTC17012, LM2015085, LM2015042 and CZ.02.1.01/0.0/0.0/16 019/0000729). We used the computing facilities SHARC, Westgrid, and Compute/Calcul Canada. Y. X. is a Tier-I Canada Research Chair in Chirality and Chirality Recognition.

Conflict of interest

The authors declare no conflict of interest.

Keywords: chirality transfer · light scattering · nickel complexes · quantum plasmons · resonance Raman optical activity

How to cite: *Angew. Chem. Int. Ed.* **2019**, *58*, 16495–16498
Angew. Chem. **2019**, *131*, 16647–16650

- [1] L. Pasteur, *Thèses de chimie et de physique*, Bachelier, Paris, **1847**.
[2] L. D. Barron, *Molecular Light Scattering and Optical Activity*, Cambridge University Press, Cambridge, **2004**.
[3] a) L. Nafie, *Vibrational optical activity: Principles and applications*, Wiley, Chichester, **2011**; b) J. Haesler, I. Schindelholz, E. Riguet, C. G. Bochet, W. Hug, *Nature* **2007**, *446*, 526–529.
[4] a) A. Baiardi, J. Bloino, V. Barone, *J. Chem. Theory Comput.* **2018**, *14*, 6370–6390; b) J. Šebestík, J. Kapitán, O. Pačes, P. Bouř,

Angew. Chem. Int. Ed. **2016**, *55*, 3504–3508; *Angew. Chem.* **2016**, *128*, 3565–3569.

- [5] a) S. O. Pour, L. Rocks, K. Faulds, D. Graham, V. Parchaňský, P. Bouř, E. W. Blanch, *Nat. Chem.* **2015**, *7*, 591–596; b) K. Osińska, M. Pecul, A. Kudelski, *Chem. Phys. Lett.* **2010**, *496*, 86–90; c) C. Johannessen, P. C. White, S. Abdali, *J. Phys. Chem. A* **2007**, *111*, 7771–7776.
[6] M. Dudek, G. Zajac, A. Kaczor, M. Baranska, *J. Phys. Chem. B* **2016**, *120*, 7807–7814.
[7] R. Shimada, H. Kano, H. Hamaguchi, *J. Chem. Phys.* **2008**, *140*, 204506.
[8] J. Šebestík, F. Teplý, I. Čisářová, J. Vávra, D. Koval, P. Bouř, *Chem. Commun.* **2016**, *52*, 6257–6260.
[9] a) K. A. Willets, R. P. VanDuyne, *Annu. Rev. Phys. Chem.* **2007**, *58*, 267–297; b) S. Y. Ding, E. M. You, Z. Q. Tian, M. Moskovits, *Chem. Soc. Rev.* **2017**, *46*, 4042–4076.
[10] a) C. Merten, H. Li, L. A. Nafie, *J. Phys. Chem. A* **2012**, *116*, 7329–7336; b) L. N. Vidal, T. Giovannini, C. Cappelli, *J. Phys. Chem. Lett.* **2016**, *7*, 3585–3590; c) L. A. Nafie, *Chem. Phys.* **1996**, *205*, 309–322.
[11] K. D. Chapkin, L. Bursi, G. J. Stec, A. Lauchner, N. J. Hogan, Y. Cui, P. Nordlander, N. J. Halas, *Proc. Natl. Acad. Sci. USA* **2018**, *115*, 9134–9139.
[12] C. Zong, M. Xu, L. J. Xu, T. Wei, X. Ma, X. S. Zheng, R. Hu, B. Ren, *Chem. Rev.* **2018**, *118*, 4946–4980.
[13] Z. Dezhahang, M. R. Poopari, J. Cheramy, Y. Xu, *Inorg. Chem.* **2015**, *54*, 4539–4549.
[14] a) A. D. Laurent, D. Jacquemin, *Int. J. Quantum Chem.* **2013**, *113*, 2019–2039; b) H. H. Falden, K. R. Falster-Hansen, K. L. Bak, S. Rettrup, S. P. A. Sauer, *J. Phys. Chem. A* **2009**, *113*, 11995–12012.
[15] A. S. Perera, J. Thomas, M. R. Poopari, Y. Xu, *Front. Chem.* **2016**, *4*, 9.
[16] a) Y. Zhang, M. R. Poopari, X. Cai, A. Savin, Z. Dezhahang, J. Cheramy, Y. Xu, *J. Nat. Prod.* **2016**, *79*, 1012–1023; b) E. Debie, L. Jaspers, P. Bultinck, W. Herrebout, B. V. D. Veken, *Chem. Phys. Lett.* **2008**, *450*, 426–430.
[17] a) S. Yamamoto, P. Bouř, *J. Comput. Chem.* **2013**, *34*, 2152–2158; b) V. Novák, M. Dendisová, P. Matějka, P. Bouř, *J. Phys. Chem. C* **2016**, *120*, 18275–18280; c) V. Novák, J. Šebestík, P. Bouř, *J. Chem. Theory Comput.* **2012**, *8*, 1714–1720.
[18] a) P. Bouř, *J. Chem. Phys.* **2007**, *127*, 136101; b) B. G. Janesko, G. E. Scuseria, *J. Chem. Phys.* **2006**, *125*, 124704.
[19] S. Lubet, C. Herrmann, M. Reiher, *J. Phys. Chem. B* **2008**, *112*, 2218–2232.
[20] M. J. Frisch, et al., Gaussian 16, Wallingford, CT, **2016**.
[21] a) A. D. Becke, *J. Chem. Phys.* **1993**, *98*, 5648–5652; b) T. Yanai, D. Tew, N. C. Handy, *Chem. Phys. Lett.* **2004**, *393*, 51–57.
[22] J. R. Cheeseman, M. J. Frisch, *J. Chem. Theory Comput.* **2011**, *7*, 3323–3334.
[23] J. B. Foresman, T. A. Keith, K. B. Wiberg, J. Snoonian, M. J. Frisch, *J. Phys. Chem.* **1996**, *100*, 16098–16104.
[24] P. J. Hay, W. R. Wadt, *J. Chem. Phys.* **1985**, *82*, 299–310.

Manuscript received: July 30, 2019

Accepted manuscript online: August 28, 2019

Version of record online: September 13, 2019